UCLA
UCLA Previously Published Works

Title

Pt8 cluster on alumina under a pressure of hydrogen: Support-dependent reconstruction from first-principles global optimization

Permalink

https://escholarship.org/uc/item/0zs8c4x7

Journal

The Journal of Chemical Physics, 151(19)

ISSN

0021-9606

Authors

Sun, Geng
Alexandrova, Anastassia N
Sautet, Philippe

Publication Date

2019-11-21

DOI

10.1063/1.5129296

Supplemental Material

https://escholarship.org/uc/item/0zs8c4x7#supplemental

Peer reviewed

eScholarship.org Powered by the California Digital Library
University of California

Pt_8 Cluster on Alumina under a Pressure of Hydrogen: Support-dependent Reconstruction from First-principles Global Optimization

Geng Sun,[1] Anastassia N. Alexandrova*,[2, 3, a)] and Philippe Sautet*[1, 3, b)]

[1)] *Department of Chemical and Biomolecular Engineering, University of California, Los Angeles, Los Angeles, California 90095, United States*

[2)] *Department of Chemistry & Biochemistry, University of California, Los Angeles, Los Angeles, California 90095, United States*

[3)] *California NanoSystems Institute, Los Angeles, California 90095, United States*

(Dated: 28 October 2019)

Alumina supported Pt nano clusters under hydrogen environment play a crucial role for many heterogeneous catalysis applications. We conducted grand canonical genetic algorithm (GCGA) simulations for supported Pt_8 clusters in hydrogen gas environment to study the intra-cluster, cluster-support, and cluster-adsorbate interactions. Two alumina surfaces, α-$Al_2O_3(0001)$ and γ-$Al_2O_3(100)$, and two conditions T=600 °C, p_{H_2}=0.1 bar and T=25 °C, p_{H_2}=1.0 bar were considered corresponding to low and high hydrogen chemical potential μ_H, respectively. The low free energy ensemble of Pt_8 is decorated by a medium ($2 \sim 12$ H), resp. high ($20 \sim 30$ H), number of hydrogen atoms under equilibrium at low μ_H, resp. high μ_H, and undergoes different morphology transformations on the two surfaces. On α-$Al_2O_3(0001)$, Pt_8 is mostly 3D but very fluxional in structure at low μ_H and converts to open one-layer 2D structures with minimal fluxionality at high μ_H, whereas on γ-$Al_2O_3(100)$, the exact opposite occurs, and Pt_8 clusters present one-layer 2D shapes at low μ_H and switch into compact 3D shapes under high μ_H, during which the Pt_8 cluster preserves moderate fluxionality. Further analysis reveals similar Pt−Pt bond length increase when switching from low μ_H to high μ_H on both surfaces, though morphology transformations are different. Electronic structure analysis shows the existence of bonding interactions between Pt and Lewis acidic Al^{3+} sites along with the Pt−O interaction, which implies the necessity to include Al neighbors to discuss the electronic structure of small Pt clusters.

Keywords: Global optimization, Pt cluster, alumina, cluster fluxionality

[a)]Electronic mail: ana@chem.ucla.edu

[b)]Electronic mail: sautet@ucla.edu

I. INTRODUCTION

Heterogeneous catalysis plays critical roles in many important industrial processes, which produce valuable chemicals. In several of these processes, supported metal clusters and nanoparticles are used as catalysts, where the clusters/nanoparticles are the active components, and high surface area materials are used as supports.[1–3] Usual support materials are metal oxides, such as alumina or silica. Oxide supports are primarily used for stabilizing metal clusters, but extensive studies also show that the oxide can influence the catalytic properties of metal clusters[4]. On the other hand, the catalyst is interacting with the reactants at operating temperatures. The reactant can adsorb on the metal clusters and modify their geometrical and electronic structures, forming the real active phase which can be different from the initial material placed in the reactor, and such a structure transition usually takes place at the reaction induction period.[5,6] Therefore, the metal clusters, the oxide supports, and the reactants constitute the basic components for the formation of the catalytic active site, and understanding their mutual interactions is required.

The supports play particularly an important role in governing the catalytic properties when subnanometer size metal clusters are considered.[7–9] In general, metal oxides used as supports in catalysis can be classified as non-reducible (e.g. Al_2O_3 and SiO_2) and reducible oxides like (e.g. CeO_2 and TiO_2). Reducible oxides are characterized by easily accessible changes in the surface stoichiometry, forming oxygen vacancies, and then interact differently with supported metal clusters. For example, it is known that in reducing conditions, metal clusters can even be buried by the reduced TiO_{2-x}.[10] This phenomenon is referred to as the strong metal-support interaction.[11–13] The non-reducible metal oxide are more stable at catalytic conditions, though that does not mean they are inert in catalytic reactions. Firstly, the unsaturated Al cations on alumina show strong Lewis acidity[14] which is important for many catalytic reactions such as hydrocarbon cracking, biomass reformation[15] etc. Secondly, the alumina prepared under different temperatures shows different crystalline phases as well as various levels of surface hydration, that also provides different properties.[16].

Under reaction conditions, metal clusters react with reactants forming the cluster-adsorbate complexes, which are the catalytically active species at steady-state conditions.[17] The cluster-adsorbates complex could be substantially different from the precursors. Since the morphology and properties of metal clusters can be altered by the adsorbate binding,

it is crucial to characterize and understand the adsorbate induced reconstructions. For example, under a CO environment, supported Rh clusters can be disintegrated into small fragments (such as Rh-$(CO)n$)[18,19] and the process is also reversible when CO is removed. This process can be completed within several seconds, which is very fast compared with the time scale in real world experiments. This means that the actual catalytic species can not be identified if the experimental characterization is conducted under vacuum and ex-situ conditions.

Sub nano Pt clusters supported on alumina in a hydrogen environment are important catalysts for many important catalytic reactions, including hydrogenation[20–22], NO_x removal[23], CO oxidation[24,25], dehydrogenation[26], and reforming[27,28]. However, these are challenging systems, because the catalytic properties of $Pt@Al_2O_3$ are sensitive to the environment, and the optimal performance requires a careful setting of reaction conditions. The chemical environment exerts a strong influence on the catalytic properties of the Pt clusters. For example, in the alkane dehydrogenation reaction, the partial pressure of the H_2 gas has a vital impact on the lifetime of the catalyst, by avoiding coking.[26] The property of the alumina support also impacts the catalytic reactions. For example, He and Wang et al. showed that the pore size distribution and the inherent acidity of Al_2O_3 change the lifetime of the catalysts.[29]. The acidity of the Al_2O_3 surface can be modified by SiO_2 or Cs_2O doping, which in turn alters the selectivity toward hydrogenolysis byproducts.[30].

Several theoretical studies investigated the effect of hydrogen adsorption on the structure and electronic properties of small Pt clusters. Those studies underlined the phenomenon of morphology transition when the environment is switched. Mager-Maury et al. investigated the morphology of Pt_{13} clusters in a wide range of hydrogen coverage. In this theoretical work, the Pt_{13} cluster is supported on the γ-$Al_2O_3(100)$ surface and the structure of $Pt_{13}H_x$ is explored by molecular dynamics.[31] The results show that at low hydrogen coverage, the Pt_{13} cluster presents a biplanar shape, but the shape converts to a cuboctahedron at high hydrogen coverage. C.H. Hu et al showed that the structure of the cluster is also affected by the choice of the alumina support. The biplanar shape of Pt_{13} on γ-$Al_2O_3(100)$, with both $Pt-O$ and $Pt-Al$ bonds, is transformed to a 3D shape, which is hydroxylated after standard temperature treatment, and the cluster only weakly interacts with the surface hydroxyl groups.[32] Another study by G.S. Erfani et al. also show that the morphology of Pt clusters on γ-$Al_2O_3(110)$ is inter-convertible by varying the surface hydroxyl coverage,[33] which alters

the strength of Pt-surface interaction. The Pt_{22} cluster shows a strong adhesion on the γ-$Al_2O_3(110)$ surface and a 2D shape at low hydroxyl coverage, while it transforms to a 3D structure when the hydroxyl coverage is greater than 0.325 ML. However, they showed that such morphological transition only takes place for the small Pt_{22} cluster and is not observed for a larger Pt_{44} cluster.[33] At finite temperature in catalytic conditions, thermal fluctuations induce cluster isomerization and formation of meta-stable structures, which are minor in the population but still accessible, and could have properties that are distinct from those of the global minimum structure.[34] Alexandrova and Anderson showed that in other applications, in the absence of added hydrogen, H-free Pt_7 and Pt_8 on α-Al_2O_3 feature 3D global minima, while Pt_7 additionally has a thermal acess to flatter isomers that wet the support, and those flat isomers (rather than the global minimum) in fact govern the catalytic activity of the system.[34,35] The shape transition is also demonstrated by experimental results from in-situ HERFD-XANES (high energy resolution fluorescence detection X-ray absorption near edge structure).[36] H. Mistry and B. R. Cuenya et al studied the electronic and structural properties of Pt clusters on γ-$Al_2O_3(100)$ under different hydrogen pressure. They found that when the partial pressure of H_2 increased from 1 to 21 bar, the H/Pt ratio changes from 1.9 to about 2.5 with a morphology transition from 2D to 3D.[37]

The present contribution follows such efforts to understand and rationalize the effect of supports and hydrogen environment on the electronic and morphological properties of Pt nano-clusters. Small Pt clusters are very flexible in geometry[35,38–43] and their global minimum and other lowest-energy accessible isomers can not be simply guessed. Additionally, hydrogen adsorption also alters the cluster' geometries, further complicating the structure identification. Therefore, we exploited a grand canonical genetic algorithm method, which optimizes the geometry and adsorbate coverage simultaneously for supported Pt_8 clusters. These simulations produce structures that are quasi-free energy minima, in the sense that they take into account the internal electronic energies of the systems, and the change of the chemical potential of hydrogen upon adsorption. For simplicity, the vibrational entropy is not accounted. We furthermore characterize the cluster systems not in terms of just one global minimum, but as ensembles of many thermally-accessible structural states. It has been shown recently that these higher-energy states are critical in determining the properties of cluster catalysts.[34,35,41–44]

In order to investigate the influence of the hydrogen environment, two different conditions

were considered in this work. The first one (T=600 °C and p_{H_2}=0.1 bar) corresponds to the standard propane dehydrogenation condition, in which hydrogen is co-fed with propane to prevent coke formation. We refer to it as the low μ_H because of the high T and low p_{H_2}. The second one (T=25 °C and p_{H_2}=1 bar) is close to a typical hydrogenation reaction and we refer to it as high μ_H in the text. In addition, two different surfaces are modeled, e.g. γ-Al_2O_3(100) and α-Al_2O_3(0001), and they are examples of surfaces with different activities due to the different Lewis acidity and basicity.

This manuscript is organized as follows. In section II, we present calculation details and the grand canonical genetic algorithm (GCGA) used in this work. Then in section III, we discuss the structures obtained with GCGA and the influence of the support surface and the hydrogen reactant on the cluster structure. Finally, In section IV, we discussed the geometry transitions and the electronic structures of supported Pt_8H_x clusters under different conditions.

II. METHODS AND MODELS

A. Grand canonical genetic algorithm

Since the hydrogen coverage of small Pt cluster varies strongly upon temperature and hydrogen pressure, determining the structure of the Pt_nH_x cluster in specific conditions is challenging. The standard approach is to explore each coverage x independently and then evaluate the phase diagram based on the optimal geometry at different composition. This approach has two major limitations. First, it is based on a single global minimum structure, whereas we now know that this representation is far from the reality at catalytic temperatures. In fact, more realistic "hot" phase diagrams based on ensembles of many accessible states have been recently introduced.[45] Secondly, one needs to perform all x global optimizations for every n in Pt_nH_x, i.e. tens of costly simulations for every single system. Considering the large system size, this approach is not practical. Therefore, we investigated the structures of supported Pt_8H_x clusters in the presence of a hydrogen reservoir by grand canonical genetic algorithm (GCGA). GCGA is a global optimization method designed for structural exploration at a fixed chemical potential rather than a fixed composition. Similar methods have been applied to explore the Zr–Cu–Al alloy with an empirical force field, 2D

materials, etc.[46]

The GCGA algorithm works similarly to the conventional GA[47,48](or evolutionary algorithm) but aims at optimizing the free energy of the target system rather than the potential energy, i.e. minimizing ΔG in Eq. 1.

$$\Delta G = E(\mathrm{Pt_8H_x + slab}) - E(\mathrm{slab}) - 8E^{\mathrm{atom}}_{\mathrm{Pt}} - x\mu_{\mathrm{H}} \tag{1}$$

where, $E(\mathrm{Pt_8H_x + slab})$ is the electronic energy of optimized structure, $E(\mathrm{slab})$ is the energy of the optimized slab model, $E^{\mathrm{atom}}_{\mathrm{Pt}}$ is the energy of free Pt atom and μ_{H} is the chemical potential of the hydrogen in the gas phase. μ_{H} is then calculated by Eq. 2[31]

$$\mu_{\mathrm{H}}(T,p) = \frac{1}{2}\left[G^0_{H_2}(T) - h^{0K} + k_B T \ln\left(\frac{p}{p^0}\right)\right] \tag{2}$$

where, T and p are the temperature and partial pressure of hydrogen. $G^0_{H_2}(T)$ is the standard free energy of H_2 at T. h^{0K} is the enthalpy correction of H_2 at 0 K, and k_B is the Boltzmann constant.

GCGA consists of several components, some of which are the same as conventional GA and others are altered for the current grand canonical (GC) approaches. The first element is the structure evolution algorithms, which includes two categories of operations: the mating (or heredity) and mutation. The mating operation generates one offspring structure from two parent structures. A detailed technical implementation of the mating operation with fixed composition can be found elsewhere.[47] In the GC approach, the algorithm needs to be modified, because the two parents may have different stoichiometries (i.e. different numbers of hydrogen atoms). In our implementation, an offspring structure is first generated from two parents as if there were no hydrogen atoms in the system. Secondly, according to the original connectivity matrix of the parent structure, hydrogen atom is also inherited to the offspring structure if one of the H binding sites (Pt atoms) was inherited. In some cases, the inherited hydrogen atoms will overlap with other H or Pt atoms in the generated structures. These overlapping hydrogen atoms are removed before optimizations. In this way, the final offspring candidate may have different coverage from its two parents. However, the bonds between H atoms and their anchoring Pt atoms are still conserved and inherited from the parents.

The mutation operation in GA usually consists in several methods to change the positions of atoms, including a) random displacement, and b) reflection with mirror symmetry. Two

additional operations are introduced in the current GCGA method. They are c) adding and d) removing one adsorbate (hydrogen in this case). The *Adding* operation is completed by inserting an additional hydrogen atom in the vicinity of a randomly selected Pt atom while avoiding the overlap with other atoms within $0.7 \times (r_i + r_j)$ (r_i is the covalent radius of atom i). The *removing* operation consists in randomly deleting a hydrogen atom from the system.

Some other elements of GA, such as the evaluation of the fitness and the determination of identical structures, follow the algorithm similar to the one introduced by Vilhelmsen et al.[47] The method exploited in this contribution is developed based on the atomic simulation environment (ASE) package. A blueprint of the GCGA is shown in the Fig. S1. Initially, structures (called seeds) are randomly generated on the slab support; typically they have high free energies (defined in Equ. 1). Hydrogen coverage is also randomly selected and hence not expected to be optimal. During the GCGA optimization, the number of hydrogen atoms, and the free energy of the system evolve simultaneously until convergence.

B. Models and DFT methods

We exploit two different crystalline alumina surfaces: α-$Al_2O_3(0001)$ and γ-$Al_2O_3(100)$, which have different surface structures. The Al^{3+} terminated α-$Al_2O_3(0001)$ contains only one type of Al site, a 3-coordinated Al cation. It is known to be the most stable surface termination in a wide range of oxygen chemical potentials (μ_O), ,and hence is used as the first model in this work. A 4×4 supercell of the α-$Al_2O_3(0001)$ with 4 Al-O-Al trilayers (total 12 atomic layers) is extracted from bulk, and optimized. During the optimization of the bare surface, the top-most layer Al^{3+} cations relax inward significantly (the inter-layer distance between Al and O becomes only 0.127 Å). The bottom two layers are then fixed at the optimized positions(from previous slab optimization) in all the following structure optimizations. The chemical formula of our α-$Al_2O_3(0001)$ slab model is $Al_{128}O_{192}$ and its structure is shown in Fig. S2(a).

The second surface is γ-$Al_2O_3(100)$, which is built from the crystalline structure reported by Digne et al.[49,50] γ-$Al_2O_3(100)$ contains two types of Al^{3+} sites, a saturated subsurface tetrahedral Al cation and a 5-coordinated and unsaturated Al cations, originating from octahedral Al in the bulk. In order to reduce the lateral interaction between different supported clusters, we used a 2×2 supercell of γ-$Al_2O_3(100)$ with the dimensions of 16.761

Å× 16.826 Å (shown in Fig. S2(b)).

During the global optimization, we exploited two density functional theory (DFT) approaches. In the first stage, the PBE functional[51] with moderate size (double-zeta) atomic basis sets (implemented in CP2K package[52]) is used. DFT with this basis set is very efficient in computation, and therefore it enables GCGA to quickly approach an approximate ensemble of lowest-energy structures and hydrogen coverages. However, the downside of the small basis sets is the basis sets superposition error (BSSE), which biased the predicted coverage and favors compact geometries. To mitigate the impact of BSSE, the molecularly optimized basis sets (MOLOPT) were used within CP2K[53]. The MOLOPT basis sets are optimized to minimize the BSSE down to $\sim 0.2\,\mathrm{kcal/mol}$.

Finally, we resume and complete every GCGA run using plane waves based DFT calculations implemented in VASP. The VASP calculations exploit plane waves basis sets up to an energy cutoff of 400 eV, the PAW pseudopotentials, and the PBE exchange-correlation functional.[51] Because we use a rather large supercell, only Γ point is sampled in the reciprocal space for Brillouin zone integration. Structure optimizations are conducted with the ASE (https://wiki.fysik.dtu.dk/ase/) package using the BFGS algorithm until the maximum residual force is below $0.02\,\mathrm{eV/Å}$ in each local optimization.

III. RESULTS AND DISCUSSION

A. Structures of $Pt_8Hx@\alpha$-$Al_2O_3(0001)$ at low μ_H

In the first two sections, we explore the structure of Pt_8H_x at low μ_H. In total, we have obtained 2756 unique structures for the $Pt_8H_x@\alpha$-$Al_2O_3(0001)$ system and 1330 unique structures for the $Pt_8H_x@\gamma$-$Al_2O_3(100)$ case. The two global minimum (GM) structures for these two systems are shown in Fig. 1 and many other structures in the low free energy ensemble (LFEE), defined as the all the sampled unique structures within 0.5 eV free energy interval from the the GM, are given in the supporting information (Fig. S4). The hydrogen coverages of the GMs are $Pt_8H_4@\alpha$-$Al_2O_3(0001)$ and $Pt_8H_5@\gamma$-$Al_2O_3(100)$ respectively.

Figure 1a and 1c show the GM structure of $Pt_8H_4@\alpha$-$Al_2O_3(0001)$, which has a pseudo 2-layer geometry. Two of the four hydrogen atoms adsorb on the bridge sites and the other two are on the top sites. The Pt_8H_4 cluster interacts with the α-$Al_2O_3(0001)$ surface through

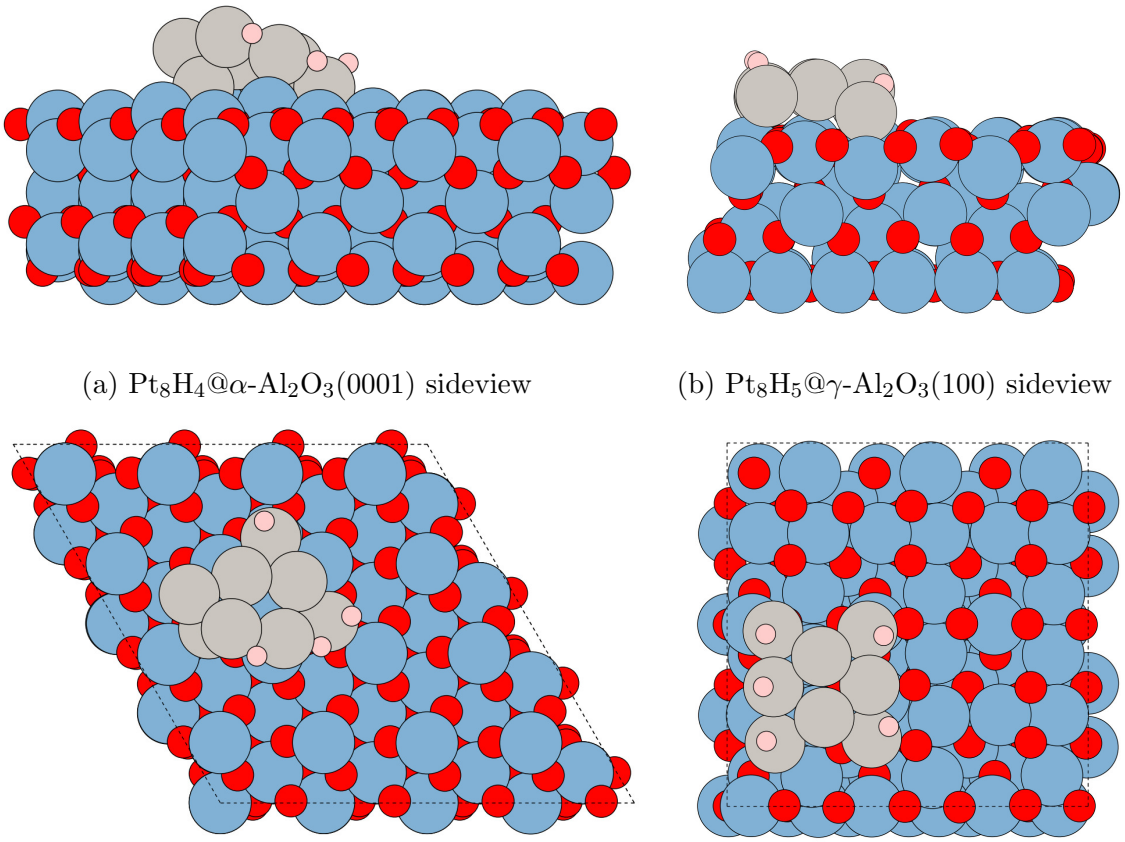

(a) Pt_8H_4@α-Al_2O_3(0001) sideview

(b) Pt_8H_5@γ-Al_2O_3(100) sideview

(c) Pt_8H_4@α-Al_2O_3(0001) topview

(d) Pt_8H_5@γ-Al_2O_3(100) topview

FIG. 1: The two global minimum structures of Pt_8H_x cluster under a pressure of hydrogen at low μ_H (600 °C and 0.1 bar of H_2). (1a) and (1c) are Pt_8H_4 supported on α-Al_2O_3(0001). (1b) and (1d) are Pt_8H_5 supported on γ-Al_2O_3(100). Red: oxygen atoms, blue: alumina atoms, gray: platinum atoms, pink: hydrogen atoms.

Pt-O bonds with 9 oxygen atoms within 2.5 Å of the cluster, and the cluster is also closely contacting at short distance ($\sim$ 2.5 Å) with 4 surface Al cations (shown in Fig. S7(a)).

To understand the interaction between the support and the cluster, the free energy of the Pt_8H_x-alumina system is decomposed into three terms including the free energy of the Pt_8H_x clusters in the absence of the substrate, the (free) energy change of support upon Pt_8H_x adsorption in the absence of the cluster and the interaction between the Pt_8H_x cluster and the deformed support. The results are shown in Fig. S8. The α-Al_2O_3(0001) of the GM structure Pt_8H_4@α-Al_2O_3(0001) undergoes rather strong deformation. Four Al^{3+} cations underneath the Pt_8H_4 cluster, which are close to Pt, stretch outward from the surface by $\sim$

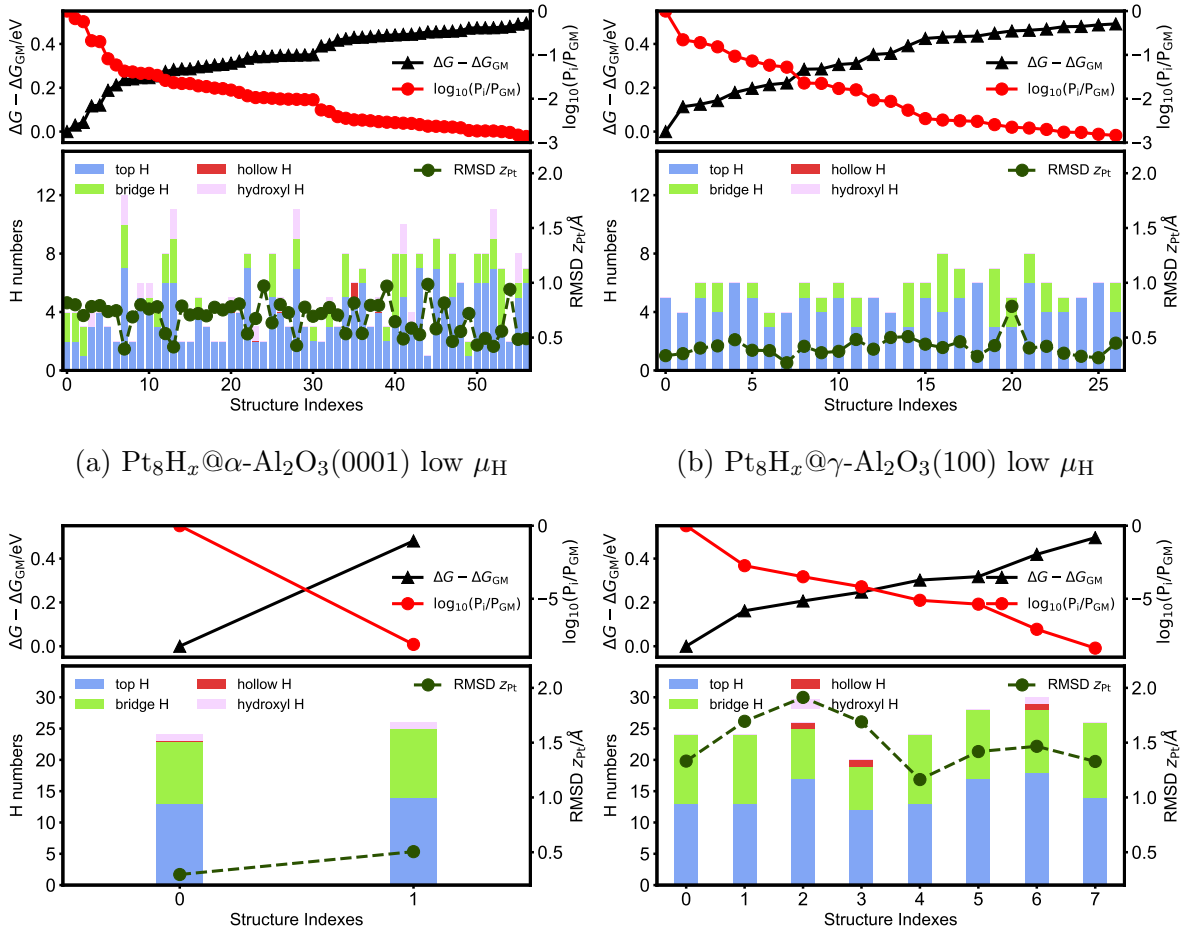

(a) Pt_8H_x@α-Al_2O_3(0001) low μ_H

(b) Pt_8H_x@γ-Al_2O_3(100) low μ_H

(c) Pt_8H_x@α-Al_2O_3(0001) high μ_H

(d) Pt_8H_x@γ-Al_2O_3(100) high μ_H

FIG. 2: Structural and energetic analysis of the low free energy ensemble for Pt_8 on alumina under a pressure of hydrogen. In each subfigure, the top panel shows the relative stability and population estimated by a Boltzmann distribution at a specific temperature. The left axis of the bottom panel shows the numbers of hydrogen atoms, which are decomposed into different types (i.e. top, bridge, hollow on Pt and hydroxyl on surface oxygen). The right axis of the bottom panel gives the RMSD of the 8 Pt atoms' heights, which is used for indicating the thickness of the cluster.

0.5 Å. This deformed structure of the surface presents, in the absence of the Pt_8H_4 cluster, an energy of 4.48 eV higher than its minimum energy. These so-called deformation energies of support in other LFEE structures are in the range of 3$\sim$ 5 eV (without hydroxyls) and 5$\sim$7 eV(with hydroxyls, shown in Fig. S8(a)).

At low μ_H and hence low H coverage, the Pt_8H_x cluster possesses a large number of low

free energy metastable isomers, as shown on Fig. 2a. In total, 57 unique structures are found for Pt_8H_x@α-Al_2O_3(0001) within 0.5 eV from the GM. Considering the high temperature ($\sim$ 600 °C), all isomers in LFEE present reasonable populations estimated by a free-energy based Boltzmann probabilities, which are larger than 0.1 % as shown in Fig. 2a, while 5 metalstable isomers show a probability higher than 10 %. The density of minima (the number of unique structures within a free energy range) is moderate around the global minimum, and it becomes larger at higher free energies. This phenomenon is similar to that of the ensemble with fixed composition. The hydrogen coverage shows large variations on the LFEE, from 1 to 12 H atoms on the cluster, and generally hydrogen atoms prefer to adsorb on either the top or bridge sites (Fig. 2c), and we did not observe any hydrogen at hollow sites. In some cases, a maximum of two hydrogen atoms can spillover to the surface forming hydroxyl. It is known that the bare α-Al_2O_3(0001) surface does not adsorb H atoms even at very high μ_H.[54,55] Therefore, as we will see later from the electronic analysis, the observed hydroxyl formation is facilitated and stabilized by the Pt_8H_x clusters. The root-mean-squired deviation (RMSD) of the eight Pt atoms' heights are analyzed to determine the shape ratio of the Pt_8H_x clusters on the support. Fig 2a shows that the RMSDs are very diverse within the LFEE, and range from 0.4 Å (flat morphology) to 1.0 Å (pseudo 2-layer shape) shown in Fig. S4. Interestingly, the planar isomers in the LFEE only appear at higher coverage($x > 8$), being accompanied with formation of surface hydroxyls. The first single layer isomer is however only 0.24 eV less stable than the GM (shown as the 8th structure in in Fig. S4), and the Boltzmann factor predicts a significant population corresponding to 7.0 % of that of the GM at 600 °C. There hence exist different morphologies for the cluster: a bilayer with low H coverage (majority shape) and a monolayer with the medium H coverage (minority shape). Distinct geometries in metastable isomers for the bare alumina supported Pt_7 cluster were previously reported by E. Baxter et al.[35]

B. Structures of Pt_8Hx@γ-Al_2O_3(100) at low μ_H

The GM structure of Pt_8H_x on γ-Al_2O_3(100) surface shows a similar hydrogen coverage (Pt_8H_5@γ-Al_2O_3(100)) compared to that on the α-Al_2O_3(0001), but a different geometry (Fig. 1b and 1d), which is an one-layer compact morphology. All five hydrogen atoms adsorb on top sites of edge Pt atoms. The Pt atoms form eight Pt−O bonds and five Pt−Al bonds

with the γ-Al_2O_3(100) surface, which is similar to the previous α-Al_2O_3(0001) surface (Fig. S7b). The GM of the Pt_8H_5 cluster however induced weaker deformation of the γ-Al_2O_3(100) than that of α-Al_2O_3(0001) surface and the γ-Al_2O_3(100) only slightly relaxed upon Pt_8H_5 adsorption. The calculated deformation energy of the γ-Al_2O_3(100) surface is 3.04 eV for GM structure (Fig. S8(b)). The stability of the isolated cluster Pt_8H_5 (indicated by its free energy), is very similar to that of isolated Pt_8H_4 on α-Al_2O_3(0001) surface, though they have different geometries and coverage. However, the interaction energy between the clusters and surfaces are much smaller on γ-Al_2O_3(100) surface (-8$\sim$-14 eV Fig. S8(b)) than that on α-Al_2O_3(0001) surface (-12 $\sim$ -20 eV shown in Fig. S8(a)). The different response of the two alumina surfaces to the cluster adsorption may originate from different surface structures and reactivity. The α-Al_2O_3(0001) contains many 3-coordinated unsaturated Al^{3+} cations, which are very Lewis acidic. However, the γ-Al_2O_3(100) surface contains only 5-coordinated unsaturated cations, which are less Lewis acidic than those of the α-Al_2O_3(0001) surface. We calculated the surface energies of the current α-Al_2O_3(0001) and γ-Al_2O_3(100) slabs (without testing the convergence of its thickness), and they are 0.118 eV/Å^2 and 0.075 eV/Å^2 respectively. The larger surface energy of α-Al_2O_3(0001) also implies its higher activity of α-Al_2O_3(0001).

The Pt_8H_x clusters on γ-Al_2O_3(100) are also fluxional at the considered low μ_H. 27 unique structures are found within the LFEE, and their relative free energies are shown in Fig. 2b. Three metastable isomers have populations larger than 10 % at the considered temperature (600 °C). The RMSDs of Pt atoms' heights show that nearly all the minima have one-layer morphologies except for just one isomer, who is a bilayer and appears at 0.46 eV above the GM (Fig. S3). The hydrogen coordination analysis shows that all the hydrogen atoms adsorb on the top or the bridge sites, and we did not observe the formation of hydroxyls in this ensemble. The distribution of H coverage is also more narrow (from 4 to 8 hydrogen atoms).

Our simulation results can be compared with the experimental work by W. Sinkler and S. Sanchez et al.[56] They studied small Pt clusters supported on γ-Al_2O_3 with aberration-corrected transmission electron microscopy. They find that the Pt clusters present a one-layer and two-dimensional morphology with a diameter around 0.88 nm after reduction at around 700 °C by H_2.[56] The clusters in this work are supposed to consist of 7-13 Pt atoms, i.e. the sizes are very similar to our calculations. The conclusions from experiments are

hence consistent with our computational results.

C. Structures of $Pt_8Hx@\alpha$-$Al_2O_3(0001)$ at high μ_H

In the case of high μ_H, we obtained 1269 unique structures for $Pt_8H_x@\alpha$-$Al_2O_3(0001)$ and 1325 unique structures for $Pt_8H_x@\gamma$-$Al_2O_3(100)$. The GM structures are shown in Fig. 3. Both of them contain 24 H atoms.

The GM structure of $Pt_8H_{24}@\alpha$-$Al_2O_3(0001)$ is shown in Fig. 3a and 3c. The Pt_8H_{24} cluster adheres very strongly to the α-$Al_2O_3(0001)$ surface, resulting in a one-layer, 2-dimensional and open morphology. One Pt atom has only one neighbor Pt, and four of them have only two Pt neighbors, with hydrogen atoms appearing at the bridge sites. The formation of hydroxyl group is also observed in the GM structure, and that is similar to some cases in the ensemble at low μ_H on α-$Al_2O_3(0001)$.

The size of LFEE in this case of high H coverage is only 2, which is much smaller than that at low μ_H case on α-$Al_2O_3(0001)$. We already observed in our previous study of isolated Pt_{13} clusters that high coverage of H adsorption was decreasing the cluster fluxionality.[34] Here, in addition, the cluster experiences a strong interaction with the supoort, freezing it even more. Though the two structures are very similar in the morphology (Fig. S6), the metastable structure is 0.48 eV higher than the GM. Considering the low temperature (25 °C) in this case, we can expect that the GM is the only observable structure. The deformation energies of the supports among these LFEE structures are about 3.9 eV (Fig. S8), which are smaller than that of the α-$Al_2O_3(0001)$ and low μ_H case, especially when compared with structures containing hydroxyls.(Fig. S8(a)) The 2-dimensional Pt_8H_{24}, if standing alone without support, is not a preferable structure in terms of the free energy due to the small number of Pt−Pt bonds (Fig. S8(c)). However, the flat geometry facilitates a large cluster-support interaction (~ -15 eV), which finally stabilizes the system.

D. Structures of $Pt_8Hx@\gamma$-$Al_2O_3(100)$ at high μ_H

The GM of $Pt_8H_x@\gamma$-$Al_2O_3(100)$ is shown in Fig. 3b and Fig. 3d. The morphology of $Pt_8H_{24}@\gamma$-$Al_2O_3(100)$ is very different from that of the GM of $Pt_8H_{24}@\alpha$-$Al_2O_3(0001)$. The Pt_8H_{24} cluster only weakly adheres to the surface forming a compact and hydrogen

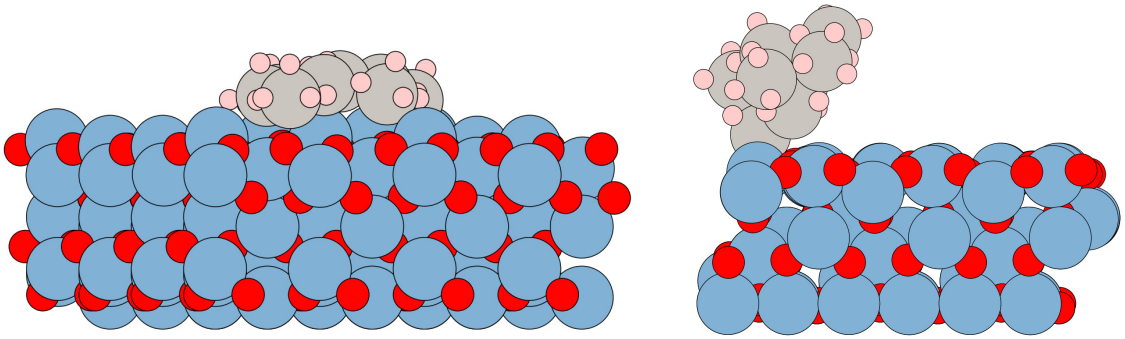

(a) Pt_8H_{24}@α-Al_2O_3(0001) sideview

(b) Pt_8H_{24}@γ-Al_2O_3(100) sideview

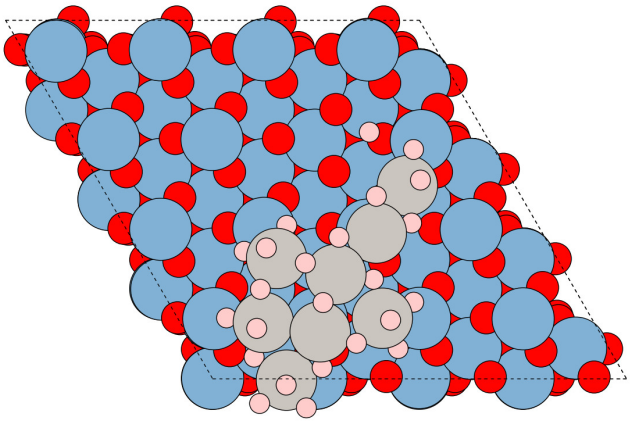

(c) Pt_8H_{24}@α-Al_2O_3(0001) topview

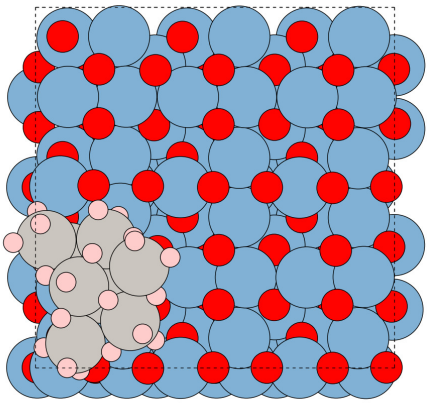

(d) Pt_8H_{24}@γ-Al_2O_3(100) topview

FIG. 3: The two GM structures of Pt_8H_x cluster. 3a and 3c are side and top view of clusters supported on α-Al_2O_3(0001). 3b and 3d are side and top view of clusters supported on γ-Al_2O_3(100). The condition refers to 25 °C and 1 bar of H_2 and the chemical formula of the clusters are Pt_8H_{24} on both surfaces. Red: oxygen atoms, blue: alumina atoms, gray: platinum atoms, pink: hydrogen atoms.

covered 3-D cluster. A single Pt atom at the bottom of the cluster interacts with a surface hollow site formed by two oxygen atoms and one Al atom. Because of the small adhesion between the cluster and γ-Al_2O_3(100), the deformation energies of γ-Al_2O_3(100) among the LFEE structures are very small (below 1.0 eV in most cases, shown in Fig. S8(d)). However, the Pt_8H_x clusters, if standalone, are much more stable than those with flat geometry on α-Al_2O_3(0001) (by more than 5.0 eV when comparing Fig. S8(c) and Fig. S8(d)).

There are 8 unique structures found in the LFEE, and all of them show a 3D morphology similar to the GM structures shown in FIG. 3b and FIG. 3d. All of them have an even count

of H adsorbates. The larger size of LFEE, compared with that of Pt_8H_x on α-$Al_2O_3(0001)$ at high μ_H, implies the cluster's fluxionality is only partially decreased by the H adsorbates due to the weak interaction between the cluster and the support(Fig. S8(d)). The hydrogen atoms still preferentially adsorb on the top or bridge sites, but some hollow sites are also occupied on the 3D clusters.

The shape transition of the Pt_8/γ-$Al_2O_3(100)$ cluster with increasing hydrogen coverage is similar to that of the Pt_{13} cluster studied by C. Mager-Maury et al.[31]. With low hydrogen coverage, both Pt_{13} and Pt_8 preferentially form compact shapes that develop a large interface with the support. With a high hydrogen coverage, both of them tend to form compact 3-D shapes with a reduced interfacial area with the support, hence maximizing the number of Pt−H bonds. The hydrogen coverage for both cluster size is also similar under the considered μ_H ($\theta \sim 3$ H/Pt at 25 °C and 1.0 bar).[31]

The support and hydrogen adsorbates hence compete for the interaction with Pt atoms, and on γ-$Al_2O_3(100)$, H atoms win. This is not the case on α-$Al_2O_3(0001)$. The energy decomposition analysis in Fig. S8 shows different driving forces to stabilize the system on each alumina surface, which result in two different reconstruction phenomena. On the α-$Al_2O_3(0001)$ surface, the interactions between the α-$Al_2O_3(0001)$ and Pt_8 clusters are overall strong, especially when the clusters present flat geometry. Under the high μ_H, the deformation of the α-$Al_2O_3(0001)$ surfaces are weakened even with flat Pt_8H_x clusters, hence the Pt_8H_x clusters prefer to retain a flat geometry under high μ_H. On the γ-$Al_2O_3(100)$, the interactions between cluster and support are generally smaller, hence dewetting and compact geometry formation prevail.

IV. DISCUSSION

A. Radial Distribution Function and Bond Lengths Relaxations

The radial distribution functions (RDFs) of Pt−Al, Pt−O and Pt−Pt are shown in FIG. 4. For each system, we compare the GM based RDF with the LFEE averaged RDF. The LFEE averaged RDF is generally similar to GM based RDF, though the former filters out some detailed RDF features. FIG. 4a shows the results of Pt_8H_x@α-$Al_2O_3(0001)$ under low μ_H hence low H coverage. Some short O−Pt distances are seen ($d \sim 2.1$ Å), which is

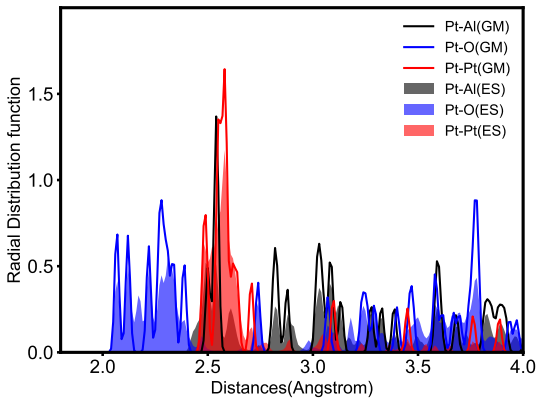

(a) Pt_8H_x@α-Al_2O_3(0001) at low μ_H

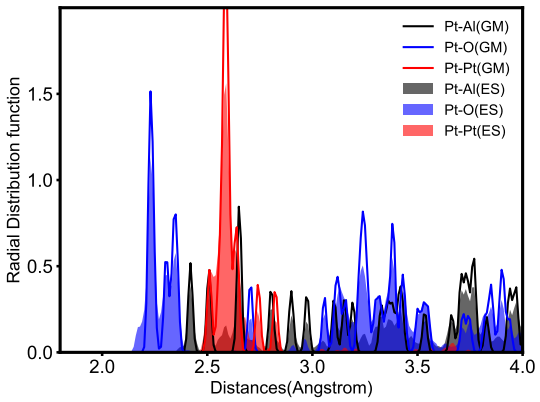

(b) Pt_8H_x@γ-Al_2O_3(100) at low μ_H

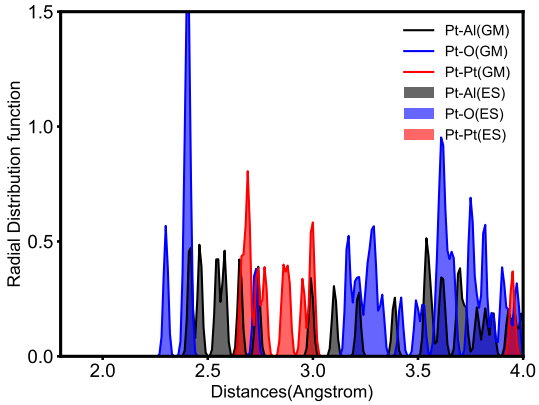

(c) Pt_8H_x@α-Al_2O_3(0001) at high μ_H

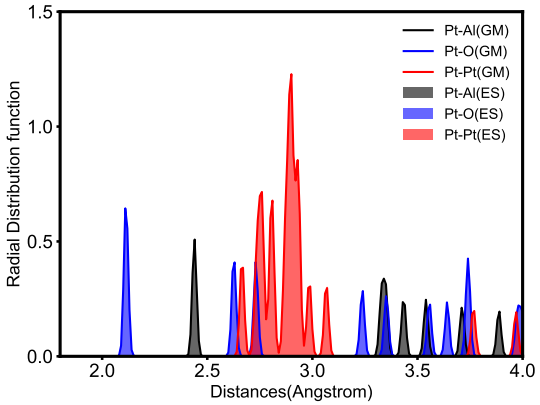

(d) Pt_8H_x@γ-Al_2O_3(100) at high μ_H

FIG. 4: Radial distribution functions for Pt−Al, Pt−O and Pt−Pt bonds respectively, in different LFEE. In each subfigure, the solid line shows the radial distribution function (RDF) evaluated only from GM structure (GM set) and the shaded area shows the RDF from averaging on the LFEE structures (ES set), with the relative weights from the Boltzmann distribution. Each RDF is Gaussian-smoothed with $\sigma = 0.05$.

;

very close to the Pt−O distance in PtO bulk (d = 2.02 Å). However, the averaged first-neighbor Pt−O distance in this system is 2.30 Å (counting all Pt−O pairs within 3.0 Å) being significantly longer than that from the bulk. The long Pt−O distance implies a weaker Pt−O interaction than that of bulk PtO. The averaged first-neighbor Al and Pt atoms are located at around 2.65 Å. This Pt−Al distance is very close to some Pt−Al alloys[57] and molecular complexes[58], but significant longer than the sum of covalent radius of

Pt and ionic radius of Al (1.9 Å). The first-neighbor Pt-Pt bond is significantly strained with smaller distance (2.57 Å) than that in Pt bulk (2.78 Å). The RDFs of Pt_8H_x@γ-Al_2O_3(100) under low μ_H show that the shortest Pt−O bonds are slightly longer than that of Pt_8H_x@α-Al_2O_3(0001), but the averaged first-neighbor distance is almost the same ($\sim$ 2.32 Å). The averaged first-neighbor Pt−Al (2.68 Å) and Pt−Pt (2.61 Å) distances are also very close to that of Pt_8H_x@α-Al_2O_3(0001).

The RDFs of structures under high μ_H cases, hence where each Pt atoms interact with several H atoms, are shown in FIG. 4c and 4d. For Pt_8H_x@α-Al_2O_3(0001), the averaged first-neighbor Pt−O bond length becomes longer (2.43 Å) than that of Pt_8H_x@α-Al_2O_3(0001) under low μ_H implying a decreased interaction between Pt and O. The Pt−Pt bonds also become longer and more diverse. The averaged first-neighbor Pt−Pt bond length is around 2.79 Å, which is almost 0.2 Å longer than that of the Pt_8H_x@α-Al_2O_3(0001) under low μ_H. In contrast to the Pt−O and Pt−Pt bonds, the first-neighbor Pt−Al bonds do not change a lot and the averaged first-neighbor Pt−Al is 2.59 Å. Some Pt−Al distances slightly decrease below 2.5 Å and others slightly increase. For Pt_8H_x@γ-Al_2O_3(100), it is recalled that the Pt_8H_x clusters form very compact geometries and only weakly adhere to the γ-Al_2O_3(100) surface with a few Pt−Al and Pt−O bonds. The Pt−Pt bond length for this system is around 2.84 Å, which is similar to that of Pt_8H_x@α-Al_2O_3(0001) under high μ_H but much longer than those clusters under low μ_H. Under the high μ_H with low low temperature $T = 25$ °C, GM play the dominating role in the LFEE averaged RDF, and metastable isomers have very small probabilities, therefore, the GM based RDF and the LFEFF averaged RDF are basically identical in the FIG. 4c and FIG. 4d. The contraction of Pt−Pt bond lengths with increasing temperature for small supported Pt clusters has been reported in the experiments of Kang, J.H. et al.[59] They find that in the presence of H_2, the Pt−Pt bond lengths of Pt clusters (d=0.9 nm) will decrease at higher temperature (e.g. at a lower μ_H). This phenomenon is also verified from our simulation results. In addition, our results reveal that the changes of the bond lengths take place with different cluster reconstructions. On the α-Al_2O_3(0001) and with increased hydrogen coverage (higher μ_H and lower T), Pt_8H_x cluster prefers to strengthen its interaction with the α-Al_2O_3(0001) surface and wet the surface. The first-neighbor Pt−Pt becomes longer during this reconstruction. On the other hand, γ-Al_2O_3(100) supported Pt_8H_x clusters are flat at low μ_H with contracted Pt−Pt bond lengths. With high μ_H, the clusters become compact 3D morphology and Pt−Pt bond

lengths become longer during the reconstruction. Although the reconstruction processes are surface dependent, the variation trend of first neighbor Pt−Pt bond lengths is common, and naturally linked with bond order conservation principle.

B. Bader charges and charge differences

The Bader charges analysis of the LFEE is shown in Fig. 5 with different conditions and surfaces. The Bader charges of hydrogen atoms (q(H_x)), Pt clusters (q(Pt_8)) and the Bader charges changes of surface Al (Δ q(Al_n)) and O (Δ q(O_m)) atoms are shown for each structure as a function of its stability order in the specific LFEE.

Fig. 5a shows the Bader charges for LEFE under low μ_H on α-Al_2O_3(0001). The Pt_8 clusters in this LFEE are always negatively charged holding $0.8\,e$ to $1.8\,e$ in total, resulting from electronic donation by the support. The amount of charge transfer has a strong correlation with the formation of surface hydroxyls. When surface hydroxyls are present, the Pt_8 cluster plays the role as an electron, withdrawing electrons released by the formation of the proton spillover. This explains the reasonable stability of a few OH groups in the presence of the cluster. If reducible oxides, such as TiO_2, are used as support, the support reduction could be an alternative mechanism to accommodate the transferred electrons.[60] The hydroxyl formation increases the surface deformation energy slightly (around $1 \sim 2$ eV larger than that of unhydroxlated surface), but strengthens the interaction between the Pt_8H_{x-1} (or Pt_8H_{x-2}) clusters and the hydroxylated surface (~ 5 eV stronger than others shown in Fig. S8(a)). In contrast to the negatively charged Pt_8, the hydrogen atoms (excluding those from hydroxyl groups) are overall neutral. The surface (i.e. α-Al_2O_3(0001)) overall donates electrons to the Pt_8H_x clusters, and these electrons mainly come from the O atoms of the supports. The Al^{3+} cations in contrast receive electronic charge from the Pt atoms, as a result of the Lewis-base/Lewis-acid interaction. This partial electron transfer towards surface Al^{3+} cations is also accompanied by the surface relaxation upon cluster adsorption. Compared with the bare surface, Al^{3+} cations relax outward by 0.5 Å forming longer Al−O bonds.

At low μ_H and on γ-Al_2O_3(100) surface (Fig 5b), the charge transfer between the surface and Pt_8H_x clusters is less significant than that of Pt_8H_x@α-Al_2O_3(0001). The total amount of negative charge that Pt_8 clusters accept is almost constant for all the structures in LFEE,

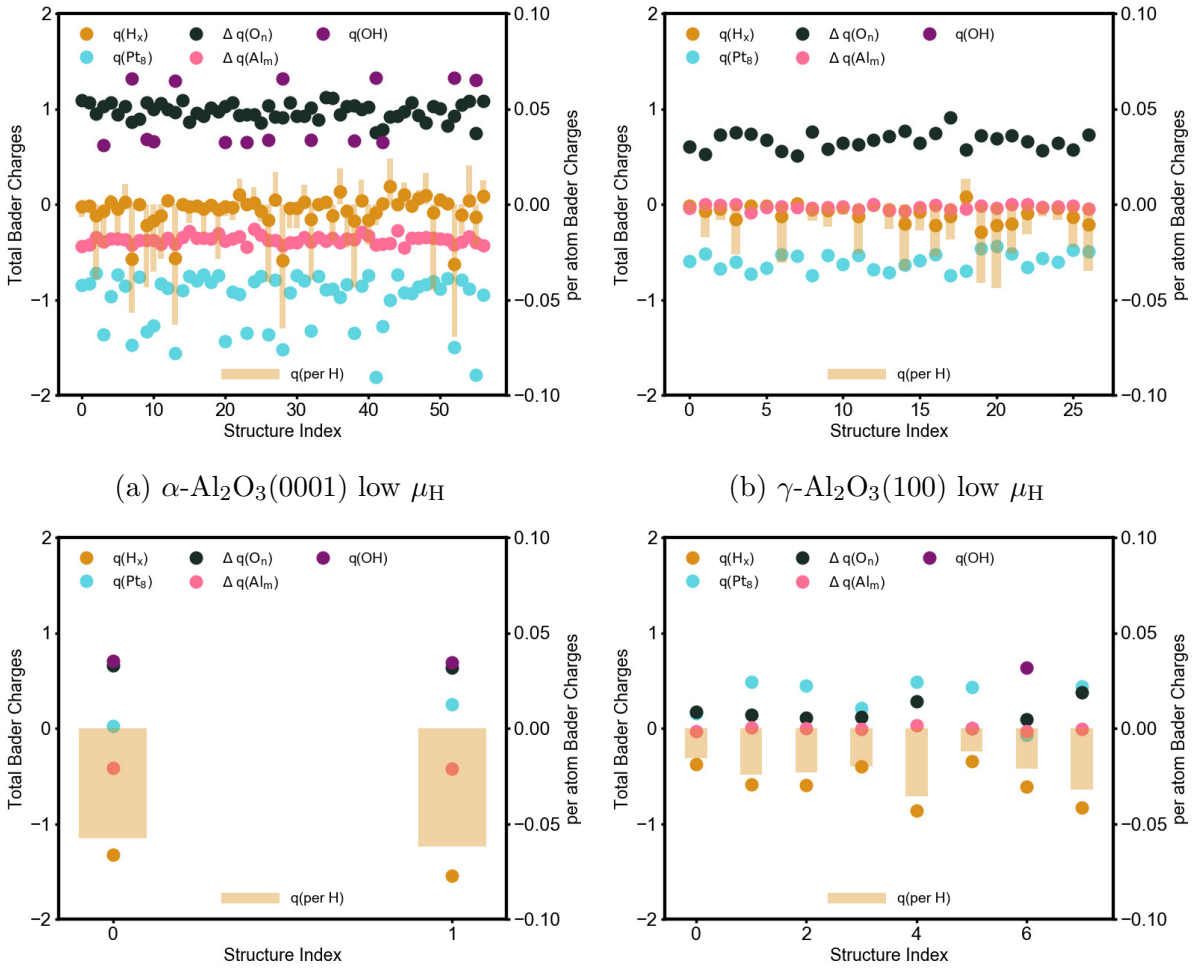

(a) α-$Al_2O_3(0001)$ low μ_H

(b) γ-$Al_2O_3(100)$ low μ_H

(c) α-$Al_2O_3(0001)$ high μ_H

(d) γ-$Al_2O_3(100)$ high μ_H

FIG. 5: Bader charges analysis on the low free energy ensemble of Pt_8H_x cluster at high and low μ_H conditions, on α-$Al_2O_3(0001)$ and γ-$Al_2O_3(100)$ surfaces. q(H_x) is the total charges of all the hydrogen atoms (except for those forming hydroxyls), q(Pt_8) is the total charges of eight Pt atoms. Δ q(O_n) and Δ q(Al_m) indicate the changes of the O and Al Bader charges upon Pt_8H_x adsorption on the support, and only the first neighbor O or Al atoms are considered. q(OH) is the Bader charges of those H atoms from hydroxyl groups. Since different clusters may contain a different number of hydrogen atoms, the per hydrogen Bader charge (excluding H in hydroxyl groups) is also shown.

ranging from -0.5 to -0.75. Again, H atoms only show a very small negative charge, smaller than $0.2\,e$ in total. The surface is also less affected than α-$Al_2O_3(0001)$. Oxygen atoms donate a fraction of electronic charge to the Pt_8H_x clusters, but the charge transferred

to Al^{3+} cations is almost zero for all the LFEE structures. This is indicative of the weaker Lewis acid character of the γ-$Al_2O_3(100)$ surface compared to α-$Al_2O_3(0001)$ surface.

At high μ_H and hence high H coverage ($\theta \sim 3.0$) on the α-$Al_2O_3(0001)$ surface, although the negative charge per H atom remains small ($0.06\,e$), the total charge present in the 23 H atoms (excluding H in hydroyxl) becomes significant ($1.4\,e$). As a results, the Pt part of the cluster becomes nearly neutral, despite the electronic donation from the surface O atoms and from the presence of a spilled over proton. Similarly to the case at low μ_H on α-$Al_2O_3(0001)$, electronic charge is transferred to the first-neighbour Al^{3+} cations. The electronic charge transfers at high μ_H on the γ-$Al_2O_3(100)$ surface are very different because the cluster dewets from the oxide and forms only one Pt−Al and/or one Pt−O bond depending on isomers. As a result, the electronic donation from O atoms is much smaller. Surface Al cations are not affected, as it was already the case at low H coverage on that support. Hence the charge transfers take place only among the Pt atoms and hydrogen atoms in most of the isomers, the Pt cluster becomes partially positively charged (up to 0.4 in the LFEE), except in one case where a H atom spills over to the support and transfers electronic charge to the cluster.

The charge transfers between the Pt_8H_x clusters and alumina surfaces are also analyzed by the electronic density difference plots($\Delta\rho$), from the difference between the sum of isolated Pt_8H_x and surface ($\rho_{PtH} + \rho_S$), and the whole supported system (ρ_{PtH-S}). The results are shown in FIG. 6. The interactions between the Pt_8H_x cluster and the alumina surface induce significant electronic charge density accumulation between nearly all the neighboring Pt−Al pairs, while the change of the charge density between close Pt-O pairs are subtle, the Pt−O bond resulting instead in a polarization of the Pt and O atoms. For the GMs of Pt_8H_4@α-$Al_2O_3(0001)$, Pt_8H_5@γ-$Al_2O_3(100)$ and Pt_8H_{24}@α-$Al_2O_3(0001)$, we also demonstrated two sliced charge difference plots for each structure. One of the two slices shows the electronic density differences between selected Pt−O pairs and another one shows the electronic density difference between selected Pt−Al pairs. The results are shown in Fig. S10-S12. The sliced electronic density difference plots show that the electronic density between Pt−O is only weakly increased (Fig. S12(f)) or even decreased (Fig. S10(f)) between Pt−O atoms on α-$Al_2O_3(0001)$ surface, while the electronic charge density is moderately increased between the Pt−O atoms on γ-$Al_2O_3(100)$ surface (Fig. S11(f)) although the increasing is less sound than that of Pt−Al bonds (Fig. S10(e), Fig. S11(e) and Fig. S12(e)). The electron localization

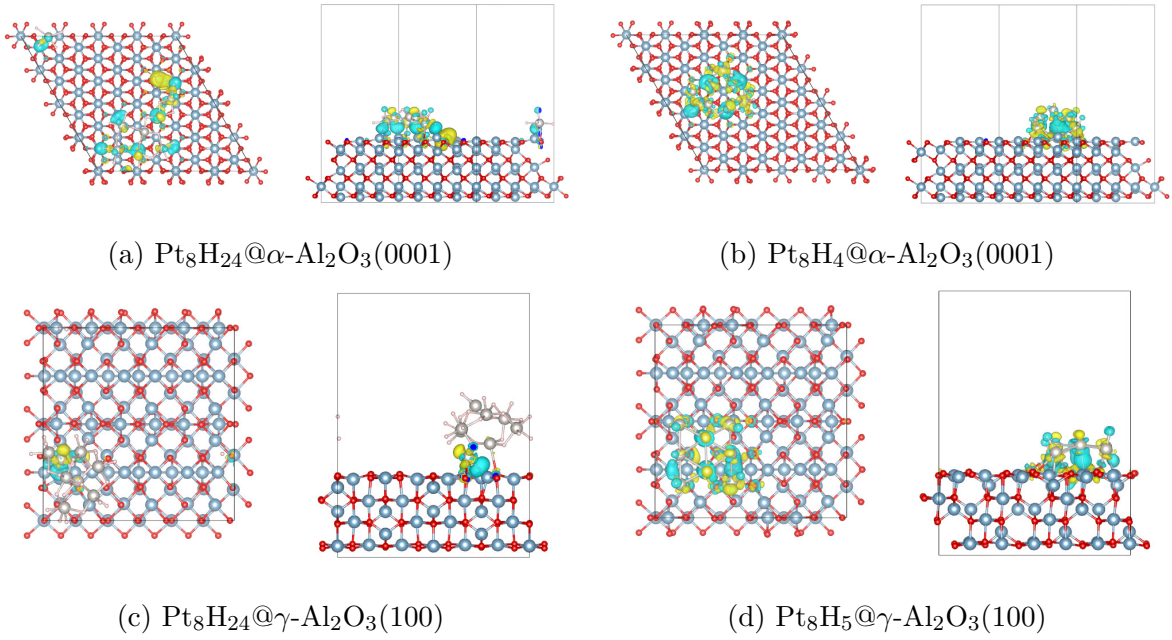

(a) Pt_8H_{24}@α-Al_2O_3(0001) (b) Pt_8H_4@α-Al_2O_3(0001)

(c) Pt_8H_{24}@γ-Al_2O_3(100) (d) Pt_8H_5@γ-Al_2O_3(100)

FIG. 6: The isosurface ($\delta = 0.005$) plot for the charge difference analysis of the four GM structures. The charge difference is defined as $\rho_{\mathrm{PtH}} + \rho_{\mathrm{S}} - \rho_{\mathrm{PtH-S}}$, where ρ_{PtH}, ρ_{S} and $\rho_{\mathrm{PtH-S}}$ are charge densities of separated cluster, separated support and all system respectively. The regions with blue (yellow) color indicates the electron density is increased (decreased) in this region.

functions are also plotted alongside with the sliced charge differences, and they are shown in Fig. S10(b-c), Fig. S11(b-c) and Fig. S12(b-c). The results demonstrate similar the bond formation between Pt – Al pairs.

C. Crystal Orbital Hamilton Population and Projected Density of States

To provide additional insight on the interactions between the Pt_8H_x clusters and the two alumina surfaces, the Crystal Orbital Hamilton Population (COHP) analysis is carried out with the LOBSTER[61–63] package. The COHP analysis is carried out for pairs of Pt – Al or Pt – O atoms when their distances are smaller than 3.5 Å. Afterwards, the COHP is plotted by accumulating all the pairs with the same elements. The projected density of states (PDOS) plots are also shown alongside with the COHP to demonstrate the contributions of different elements. The results are shown in FIG. 7 for clusters on α-Al_2O_3(0001) and FIG. 8 for clusters on γ-Al_2O_3(100).

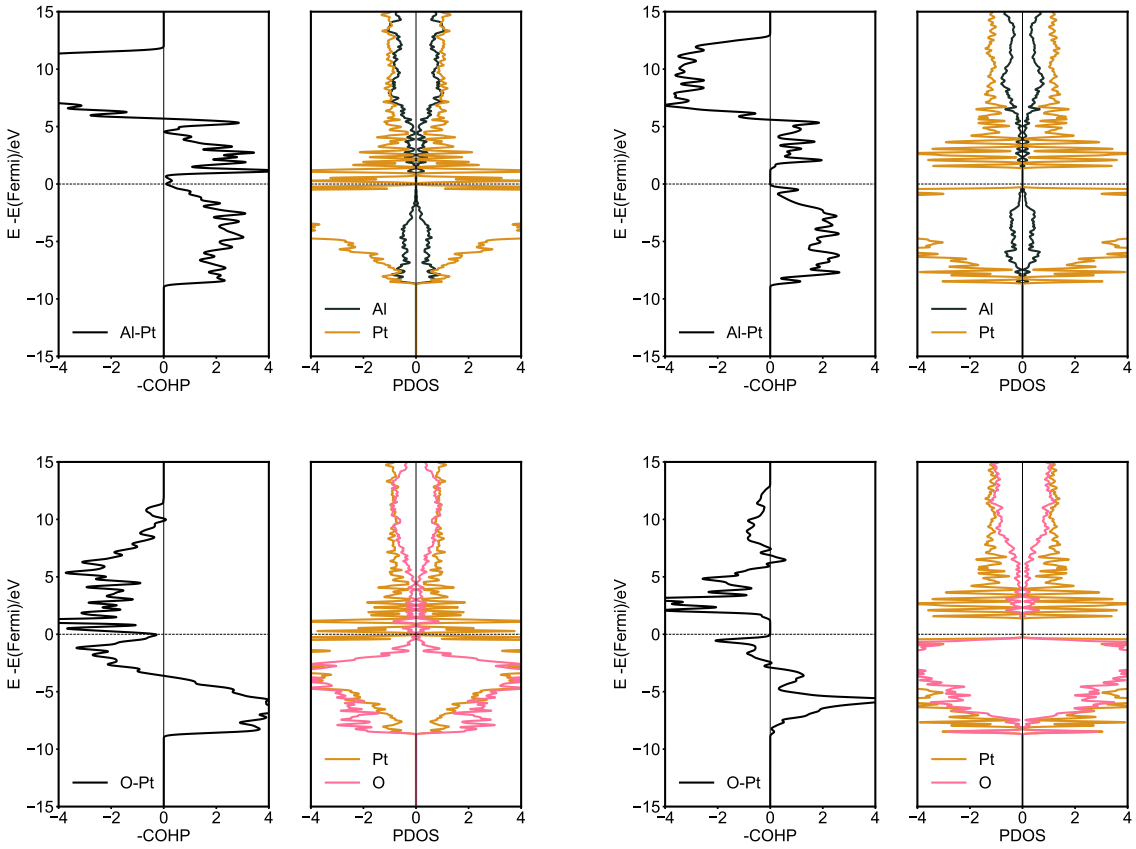

(a) Pt_8H_4@α-Al_2O_3(0001)

(b) Pt_8H_{24}@α-Al_2O_3(0001)

FIG. 7: COHP analysis of two GMs on α-Al_2O_3(0001) surface. FIG. 7a shows the results for GM Pt_8H_4@α-Al_2O_3(0001) and FIG. 7b shows the results for GM Pt_8H_{24}@α-Al_2O_3(0001).

The COHP plots of Pt_8H_4@α-Al_2O_3(0001) (FIG. 7a) show a bonding interaction between Pt and O in the first part of the occupied band (-9 to -4 eV) but the interaction then becomes antibonding in the rest of the occupied band until the Fermi level. Such a case, characteristic of an interaction between most occupied states[64] results in a decreased overall Pt$-$O overlap population, and hence weakened covalent component of the bond. Note that the interaction is still favorable since most of the antibonding states are push above the Fermi level. In contrast the Al$-$Pt interaction remains bonding on the whole range of the occupied band, in a mixing between majority Pt and minority Al orbitals. Al orbitals are indeed mainly located in the vacant part of the band (Fig. S9). The conclusion from COHP is consistent with the increased electronic charge density between Pt and Al shown in FIG.

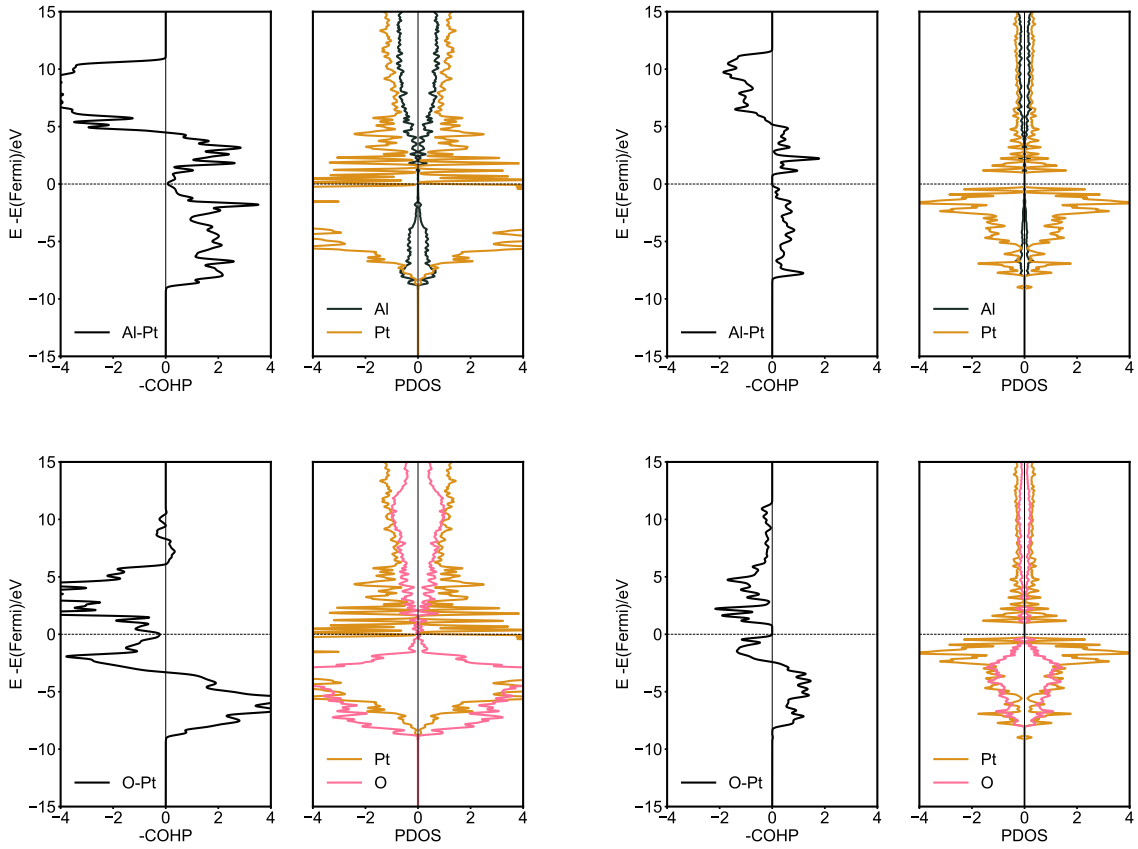

(a) Pt_8H_5@γ-Al_2O_3(100) (b) Pt_8H_{24}@γ-Al_2O_3(100)

FIG. 8: COHP analysis for the Al−Pt and O−Pt interactions of two GMs on α-Al_2O_3(0001) surface. FIG. 8a shows the results for GM Pt_8H_5@γ-Al_2O_3(100) and FIG. 8b shows the results for GM Pt_8H_{24}@γ-Al_2O_3(100).

6b. The COHP plots for the GM of Pt_8H_{24}@α-Al_2O_3(0001) surface are shown in FIG. 7b. Note that the high H coverage open a gap at the Fermi level. The overall conclusion is similar to that of Pt_8H_4@α-Al_2O_3(0001).

The COHP and PDOS of the GM Pt_8H_5 cluster on γ-Al_2O_3(100) surface are shown in FIG 8a. Again, a bonding interaction is seen between the neighboring Pt−Al pairs on the whole occupied energy range, while both bonding and antibonding energy ranges exist for Pt−O pairs. For the Pt_8H_{24}@γ-Al_2O_3(100), the population of Al orbitals in bonding interactions is minimal, which results from the rather small adhesion of the cluster on γ-Al_2O_3(100) surface. The − COHP of each case is integrated for all the occupied orbitals, including both bonding and antibonding populations, and shown in Fig. S13. The integrated numbers

provide similar insight that Pt−Al contributes to the surface-cluster interaction alongside with Pt−O.

On both surfaces, it is found that Pt_8 clusters with small hydrogen coverage retain the metallic nature with reasonable density of states around the E_f, this is a indication of their potential good catalytic activity. Therefore, the small Pt clusters can be used for reactions at high temperature, such as propane dehydrogenation.[65] However, the large hydrogen coverage ($\theta \sim 3.0$) under the high μ_H results in a closed-shell electronic structure with a rather large band gap ($\sim 1.5\,eV$) on both surfaces (shown in Fig. S9(b) and Fig. S9(d)). This implies that the considered GM Pt_8H_{24} cluster could be potentially not active in such a hydrogen environment. The potential activity can be achieved by dynamically detaching hydrogen atoms to create metastable structures,[34] which will be addressed in our further studies.

V. CONCLUSION

In this manuscript, we exploited density functional theory based grand canonical genetic algorithm to explore the ensemble of low free energy structures for hydrogenated Pt_8 clusters on two surfaces, α-$Al_2O_3(0001)$ and γ-$Al_2O_3(100)$, and in two different hydrogen chemical potentials, i.e. low μ_H (T=600 °C, p_{H_2}=0.1 bar) and high μ_H (T=25 °C, p_{H_2}=1.0 bar). We find that the different supports do not significantly change optimal hydrogen coverage on the cluster, but induce different morphology transitions. On α-$Al_2O_3(0001)$ surface, the Pt_8H_x cluster switches from a pseudo bilayer shape at low μ_H (low H coverage) to a completely flat and open structure at high μ_H (high H coverage). The strong interaction with the support is kept even at high H coverage. On the γ-$Al_2O_3(100)$ surface, in contrast, Pt_8H_x cluster shows a compact one-layer shape under low μ_H and converts to a complete globular 3D structure, in weak interaction with the support, at high μ_H and high H coverage. These morphology transitions are not only valid for GMs, but are preserved for all the low free energy clusters of the ensemble, except for the case of Pt_8H_x@α-$Al_2O_3(0001)$ at low μ_H condition, where the Pt_8H_x@α-$Al_2O_3(0001)$ shows diverse morphologies. Although Pt_8H_x undergoes different reconstructions on each support, it demonstrates on both of them a Pt-Pt bond contraction when μ_H is switched from high to low values, corresponding to a increased temperature. This observation renders a non-unique and surface dependent explanation to experimental observed Pt bond lengths contraction under H_2 when temperature is increased. Electronic

analysis explains the origin of the distinct morphology change. α-Al_2O_3(0001) support develops a stronger interaction with the Pt cluster than γ-Al_2O_3(100), as seen from the amplitude of charge transfer, of oxide surface relaxation at the interface, from the interfacial bond-length and overlap populations. The analysis also evidences Metal-Lewis acidic (M-LA) bond formation between Pt and Al cations, in addition to well characterized Pt-O bonds, which influences the electronic structure of small Pt clusters on alumina surface. This study hence provides detailed insights on the origin and strength of alumina support-Pt cluster interactions, and the consequences on the structure and coverage of small Pt clusters under a pressure of hydrogen. It can also be helpful to rationalize experiments with characterize the valence orbitals in alumina supported Pt clusters, such as X-ray absorption near edge structure.

VI. ACKNOWLEDGMENTS

This work was funded by DOE-BES grant DE-SC0019152. This work used computational and storage services associated with the Hoffman2 Shared Cluster provided by UCLA Institutefor Digital Research and Education's Research Technology Group. This research used resources of the National Energy Research Scientific Computing Center (NERSC), a U.S. Department of Energy Office of Science User Facility operated under Contract No. DE-AC02-05CH11231. An award of computer time was provided by the Innovative and Novel Computational Impact on Theory and Experiment (INCITE) program. This research used resources of the Argonne Leadership Computing Facility, which is a DOE Office of Science User Facility supported under Contract DE-AC02-06CH11357.

REFERENCES

[1]S. Tosoni and G. Pacchioni, "Oxide-supported gold clusters and nanoparticles in catalysis: A computational chemistry perspective," ChemCatChem **11**, 73–89 (2019).

[2]R. Cortese, R. Schimmenti, A. Prestianni, and D. Duca, "Dft calculations on subnanometric metal catalysts: a short review on new supported materials," Theor. Chem. Acc. **137**, 59 (2018).

[3]C. R. Henry, "Surface studies of supported model catalysts," Surf. Sci. Rep. **31**, 231–325 (1998).

[4]A. Y. Stakheev and L. Kustov, "Effects of the support on the morphology and electronic properties of supported metal clusters: modern concepts and progress in 1990s," Appl. Catal., A **188**, 3–35 (1999).

[5]D. Ma, Y. Shu, M. Cheng, Y. Xu, and X. Bao, "On the induction period of methane aromatization over mo-based catalysts," J. Catal. **194**, 105–114 (2000).

[6]H. Jiang, L. Wang, W. Cui, and Y. Xu, "Study on the induction period of methane aromatization over mo/hzsm-5: partial reduction of mo species and formation of carbonaceous deposit," Catal. Lett. **57**, 95–102 (1999).

[7]M. Ahmadi, H. Mistry, and B. Roldan Cuenya, "Tailoring the catalytic properties of metal nanoparticles via support interactions," J. Phys. Chem. Lett. **7**, 3519–3533 (2016), pMID: 27530730.

[8]C. Mager-Maury, C. Chizallet, P. Sautet, and P. Raybaud, "Platinum nanoclusters stabilized on γ-alumina by chlorine used as a capping surface ligand: A density functional theory study," ACS Catal. **2**, 1346–1357 (2012).

[9]P. Raybaud, C. Chizallet, C. Mager-Maury, M. Digne, H. Toulhoat, and P. Sautet, "From γ-alumina to supported platinum nanoclusters in reforming conditions: 10years of dft modeling and beyond," J. Catal. **308**, 328 – 340 (2013), 50th Anniversary Special Issue.

[10]H. Tang, Y. Su, B. Zhang, A. F. Lee, M. A. Isaacs, K. Wilson, L. Li, Y. Ren, J. Huang, M. Haruta, *et al.*, "Classical strong metal–support interactions between gold nanoparticles and titanium dioxide," Sci. Adv. **3**, e1700231 (2017).

[11]M. Spencer, "Models of strong metal-support interaction (smsi) in pt on tio2 catalysts," J. Catal. **93**, 216–223 (1985).

[12]S. Tauster, S. Fung, and R. L. Garten, "Strong metal-support interactions. group 8 noble metals supported on titanium dioxide," J. Am. Chem. Soc. **100**, 170–175 (1978).

[13]S. Tauster and S. Fung, "Strong metal-support interactions: occurrence among the binary oxides of groups iia–vb," J. Catal. **55**, 29–35 (1978).

[14]H. Pines and W. O. Haag, "Alumina: catalyst and support. i. alumina, its intrinsic acidity and catalytic activity1," J. Am. Chem. Soc. **82**, 2471–2483 (1960).

[15]M. El Doukkali, A. Iriondo, J. Cambra, I. Gandarias, L. Jalowiecki-Duhamel, F. Dumeignil, and P. Arias, "Deactivation study of the pt and/or ni-based γ-al2o3 catalysts used in the

aqueous phase reforming of glycerol for h2 production," Appl. Catal., A **472**, 80–91 (2014).

[16]M. Trueba and S. P. Trasatti, "γ-alumina as a support for catalysts: a review of fundamental aspects," Eur. J. Inorg. Chem. **2005**, 3393–3403 (2005).

[17]C. Chizallet and P. Raybaud, "Density functional theory simulations of complex catalytic materials in reactive environments: beyond the ideal surface at low coverage," Catal. Sci. Technol. **4**, 2797–2813 (2014).

[18]A. Suzuki, Y. Inada, A. Yamaguchi, T. Chihara, M. Yuasa, M. Nomura, and Y. Iwasawa, "Time scale and elementary steps of co-induced disintegration of surface rhodium clusters," Angew. Chem. Int. Ed. Engl. **42**, 4795–4799 (2003).

[19]R. Ouyang, J.-X. Liu, and W.-X. Li, "Atomistic theory of ostwald ripening and disintegration of supported metal particles under reaction conditions," J. Am. Chem. Soc. **135**, 1760–1771 (2013).

[20]J. Rousset, L. Stievano, F. C. S. Aires, C. Geantet, A. Renouprez, and M. Pellarin, "Hydrogenation of toluene over γ-al2o3-supported pt, pd, and pd–pt model catalysts obtained by laser vaporization of bulk metals," J. Catal. **197**, 335–343 (2001).

[21]J. Rousset, L. Stievano, F. C. S. Aires, C. Geantet, A. Renouprez, and M. Pellarin, "Hydrogenation of tetralin in the presence of sulfur over γ-al2o3-supported pt, pd, and pd–pt model catalysts," J. Catal. **202**, 163–168 (2001).

[22]S. D. Lin and M. A. Vannice, "Hydrogenation of aromatic hydrocarbons over supported pt catalysts. i. benzene hydrogenation," J. Catal. **143**, 539–553 (1993).

[23]L. Castoldi, R. Matarrese, M. Daturi, J. Llorca, and L. Lietti, "Al2o3-supported pt/rh catalysts for nox removal under lean conditions," Appl. Catal., A **581**, 43–57 (2019).

[24]M. Kahlich, H. Gasteiger, and R. Behm, "Kinetics of the selective co oxidation in h2-rich gas on pt/al2o3," J. Catal. **171**, 93–105 (1997).

[25]M. Moses-DeBusk, M. Yoon, L. F. Allard, D. R. Mullins, Z. Wu, X. Yang, G. Veith, G. M. Stocks, and C. K. Narula, "Co oxidation on supported single pt atoms: Experimental and ab initio density functional studies of co interaction with pt atom on θ-al2o3 (010) surface," J. Am. Chem. Soc. **135**, 12634–12645 (2013).

[26]O. A. Bariås, A. Holmen, and E. A. Blekkan, "Propane dehydrogenation over supported pt and pt–sn catalysts: catalyst preparation, characterization, and activity measurements," J. Catal. **158**, 1–12 (1996).

[27]J. Shabaker, R. Davda, G. Huber, R. Cortright, and J. Dumesic, "Aqueous-phase reforming of methanol and ethylene glycol over alumina-supported platinum catalysts," J. Catal. **215**, 344–352 (2003).

[28]M. García-Diéguez, I. Pieta, M. Herrera, M. Larrubia, and L. Alemany, "Nanostructured pt-and ni-based catalysts for co2-reforming of methane," J. Catal. **270**, 136–145 (2010).

[29]S. He, C. Sun, Z. Bai, X. Dai, and B. Wang, "Dehydrogenation of long chain paraffins over supported pt-sn-k/al2o3 catalysts: A study of the alumina support effect," Appl. Catal., A **356**, 88–98 (2009).

[30]B. Schimmoeller, F. Hoxha, T. Mallat, F. Krumeich, S. E. Pratsinis, and A. Baiker, "Fine tuning the surface acid/base properties of single step flame-made pt/alumina," Appl. Catal., A **374**, 48–57 (2010).

[31]C. Mager-Maury, G. Bonnard, C. Chizallet, P. Sautet, and P. Raybaud, "H2-induced reconstruction of supported pt clusters: Metal–support interaction versus surface hydride," ChemCatChem **3**, 200–207 (2011).

[32]C. H. Hu, C. Chizallet, C. Mager-Maury, M. Corral-Valero, P. Sautet, H. Toulhoat, and P. Raybaud, "Modulation of catalyst particle structure upon support hydroxylation: Ab initio insights into pd13 and pt13/γ-al2o3," J. Catal. **274**, 99–110 (2010).

[33]G. S. Shafai, S. Hong, and T. S. Rahman, "Effects of γ-al2o3 support on the morphology and electronic structure of pt nanoparticles," J. Phys. Chem. C **123** (2019).

[34]G. Sun and P. Sautet, "Metastable structures in cluster catalysis from first-principles: structural ensemble in reaction conditions and metastability triggered reactivity," J. Am. Chem. Soc. **140**, 2812–2820 (2018).

[35]E. T. Baxter, M.-A. Ha, A. C. Cass, A. N. Alexandrova, and S. L. Anderson, "Ethylene dehydrogenation on pt4, 7, 8 clusters on al2o3: strong cluster size dependence linked to preferred catalyst morphologies," ACS Catal. **7**, 3322–3335 (2017).

[36]A. Gorczyca, V. Moizan, C. Chizallet, O. Proux, W. Del Net, E. Lahera, J.-L. Hazemann, P. Raybaud, and Y. Joly, "Monitoring morphology and hydrogen coverage of nanometric pt/γ-al2o3 particles by in situ herfd–xanes and quantum simulations," Angew. Chem. Int. Ed. Engl. **126**, 12634–12637 (2014).

[37]H. Mistry, F. Behafarid, S. R. Bare, and B. Roldan Cuenya, "Pressure-dependent effect of hydrogen adsorption on structural and electronic properties of pt/γ-al2o3 nanoparticles," ChemCatChem **6**, 348–352 (2014).

[38]L. Barrio, P. Liu, J. Rodriguez, J. Campos-Martin, and J. Fierro, "A density functional theory study of the dissociation of h 2 on gold clusters: Importance of fluxionality and ensemble effects," J. Chem. Phys. **125**, 164715 (2006).

[39]K. C. Kharas and L. F. Dahl, "Ligand-stabilized metal clusters: Structure, bonding, fluxionality, and the metallic state," Adv. Chem. Phys. , 1–43 (1988).

[40]M. Gao, A. Lyalin, M. Takagi, S. Maeda, and T. Taketsugu, "Reactivity of gold clusters in the regime of structural fluxionality," J. Phys. Chem. C **119**, 11120–11130 (2015).

[41]H. Zhai and A. N. Alexandrova, "Fluxionality of catalytic clusters: when it matters and how to address it," ACS Catal. **7**, 1905–1911 (2017).

[42]H. Zhai and A. N. Alexandrova, "Local fluxionality of surface-deposited cluster catalysts: the case of pt7 on al2o3," J. Phys. Chem. Lett. **9**, 1696–1702 (2018).

[43]H. Zhai and A. N. Alexandrova, "Ensemble-average representation of pt clusters in conditions of catalysis accessed through gpu accelerated deep neural network fitting global optimization," J. Chem. Theory Comput. **12**, 6213–6226 (2016).

[44]B. Zandkarimi and A. N. Alexandrova, "Surface-supported cluster catalysis: Ensembles of metastable states run the show," Wiley Interdiscip. Rev. Comput. Mol. Sci. , e1420 (2019).

[45]Z. Zhang, E. Jimenez-Izal, I. Hermans, and A. N. Alexandrova, "Dynamic phase diagram of catalytic surface of hexagonal boron nitride under conditions of oxidative dehydrogenation of propane," J. Phys. Chem. Lett. **10**, 20–25 (2018).

[46]W. W. Tipton and R. G. Hennig, "A grand canonical genetic algorithm for the prediction of multi-component phase diagrams and testing of empirical potentials," J. Phys.: Condens. Matter **25**, 495401 (2013).

[47]L. B. Vilhelmsen and B. Hammer, "A genetic algorithm for first principles global structure optimization of supported nano structures," J. Chem. Phys. **141**, 044711 (2014).

[48]A. N. Alexandrova, A. I. Boldyrev, Y.-J. Fu, X. Yang, X.-B. Wang, and L.-S. Wang, "Structure of the na x cl x+ 1-(x= 1–4) clusters via ab initio genetic algorithm and photoelectron spectroscopy," J. Chem. Phys. **121**, 5709–5719 (2004).

[49]M. Digne, P. Sautet, P. Raybaud, P. Euzen, and H. Toulhoat, "Use of dft to achieve a rational understanding of acid–basic properties of γ-alumina surfaces," J. Catal. **226**, 54–68 (2004).

[50]M. Digne, P. Sautet, P. Raybaud, P. Euzen, and H. Toulhoat, "Hydroxyl groups on γ-alumina surfaces: a dft study," Journal of Catalysis **211**, 1–5 (2002).

[51]J. P. Perdew, K. Burke, and M. Ernzerhof, "Generalized gradient approximation made simple," Phys. Rev. Lett. **77**, 3865 (1996).

[52]J. Hutter, M. Iannuzzi, F. Schiffmann, and J. VandeVondele, "cp2k: atomistic simulations of condensed matter systems," Wiley Interdiscip. Rev. Comput. Mol. Sci. **4**, 15–25 (2014).

[53]J. VandeVondele and J. Hutter, "Gaussian basis sets for accurate calculations on molecular systems in gas and condensed phases," J. Chem. Phys. **127**, 114105 (2007).

[54]P. J. Eng, T. P. Trainor, G. E. Brown Jr, G. A. Waychunas, M. Newville, S. R. Sutton, and M. L. Rivers, "Structure of the hydrated α-al2o3 (0001) surface," Science **288**, 1029–1033 (2000).

[55]G. Zhang, X. Wang, Y. Xiong, Y. Shi, J. Song, and D. Luo, "Mechanism for adsorption, dissociation and diffusion of hydrogen in hydrogen permeation barrier of α-al2o3: a density functional theory study," Int. J. Hydrogen Energy **38**, 1157–1165 (2013).

[56]W. Sinkler, S. I. Sanchez, S. A. Bradley, J. Wen, B. Mishra, S. D. Kelly, and S. R. Bare, "Aberration-corrected transmission electron microscopy and in situ xafs structural characterization of pt/γ-al2o3 nanoparticles," ChemCatChem **7**, 3779–3787 (2015).

[57]W. Bronger and K. Wrzesien, "The structure of al3pt5," J. Alloys Compd. **244**, 194–196 (1996).

[58]M. Devillard, R. Declercq, E. Nicolas, A. W. Ehlers, J. Backs, N. Saffon-Merceron, G. Bouhadir, J. C. Slootweg, W. Uhl, and D. Bourissou, "A significant but constrained geometry pt-al interaction, fixation of co2 and cs2, activation of h2 and phconh2," J. Am. Chem. Soc. **138**, 4917–4926 (2016).

[59]J. H. Kang, L. D. Menard, R. G. Nuzzo, and A. I. Frenkel, "Unusual non-bulk properties in nanoscale materials: thermal metal- metal bond contraction of γ-alumina-supported pt catalysts," J. Am. Chem. Soc. **128**, 12068–12069 (2006).

[60]H.-Y. T. Chen, S. Tosoni, and G. Pacchioni, "Hydrogen adsorption, dissociation, and spillover on ru10 clusters supported on anatase tio2 and tetragonal zro2 (101) surfaces," ACS Catal. **5**, 5486–5495 (2015).

[61]V. L. Deringer, A. L. Tchougréeff, and R. Dronskowski, "Crystal orbital hamilton population (cohp) analysis as projected from plane-wave basis sets," J. Phys. Chem. A **115**, 5461–5466 (2011).

[62]S. Maintz, V. L. Deringer, A. L. Tchougréeff, and R. Dronskowski, "Analytic projection from plane-wave and paw wavefunctions and application to chemical-bonding analysis in

solids," J. Comput. Chem. **34**, 2557–2567 (2013).

[63]S. Maintz, V. L. Deringer, A. L. Tchougréeff, and R. Dronskowski, "Lobster: A tool to extract chemical bonding from plane-wave based dft," J. Comput. Chem. **37**, 1030–1035 (2016).

[64]R. Hoffmann, "A chemical and theoretical way to look at bonding on surfaces," Rev. Mod. Phys. **60**, 601 (1988).

[65]J. J. Sattler, J. Ruiz-Martinez, E. Santillan-Jimenez, and B. M. Weckhuysen, "Catalytic dehydrogenation of light alkanes on metals and metal oxides," Chem. Rev. **114**, 10613–10653 (2014).